Random adaptive tool path for zonal optics fabrication

VIPENDER SINGH NEGI,[1,2] **TIANYI WANG,**[3] **HARRY GARG,**[1,2] **WESLIN C. PULLEN,**[4] **XIAOLONG KE,**[5] **SHRAVAN KUMAR RR,**[1] **HEEJOO CHOI,**[4,6] **UMESH KUMAR TIWARI,**[1,2,8] **VINOD KARAR,**[1] **AND DAEWOOK KIM**[4,6,7,*]

[1]*Council of Scientific and Industrial Research-Central Scientific Instruments Organisation (CSIR-CSIO), Chandigarh- 160030, India*
[2]*Academy of Scientific and Innovative Research (AcSIR), Ghaziabad- 201002, India*
[3]*National Synchrotron Light Source II (NSLS-II), Brookhaven National Laboratory, PO Box 5000, Upton, New York 11973, USA*
[4]*James C. Wyant College of Optical Sciences, University of Arizona, 1630 E. University Blvd., Tucson, Arizona 85721, USA*
[5]*School of Mechanical and Automotive Engineering, Xiamen University of Technology, Xiamen 361024, China*
[6]*Large Binocular Telescope Observatory, University of Arizona, Tucson, Arizona 85721, USA*
[7]*Department of Astronomy and Steward Observatory, University of Arizona, 933 N. Cherry Ave., Tucson, Arizona 85721, USA*
[8]*umeshtiwari@csio.res.in*
[*]*dkim@optics.arizona.edu*

Abstract: Deterministic optics fabrication using sub-aperture tools has been vital for manufacturing precision optical surfaces. The fabrication process requires the tool influence function and the tool path to calculate the dwell time that guides the tool to bring surface quality within tight design tolerances. Widely used spiral and raster paths may leave excess waviness from the tool path, and the unavoidable constant removal layer is added to obtain positive dwell time. This waviness can be removed by either using smaller tools sequentially or randomizing the tool path. However, the existing tool-path solutions can hardly adapt to different surface aperture shapes and localized surface errors. Process efficiency and accuracy are also not well considered in tool-path planning. We propose an innovative zonal Random Adaptive Path (RAP) to solve these problems in this study. Firstly, RAP can be flexibly adapted to different surface aperture shapes by introducing part boundary. Secondly, an average threshold strategy is used in the RAP planning to improve efficiency, enabling the surface errors to be selectively corrected. Finally, the threshold is performed in several passes within one processing cycle, each with its RAP, until the desired residual is achieved. The performance of the proposed RAP is studied by comparing it with the conventional tool paths. The results demonstrated that RAP takes the least processing time and achieves the best surface quality, which verifies the effectiveness of RAP in deterministic optics fabrication.

1. Introduction

Tailored optical components have essential applications in space exploration, consumer products, surveillance, and health care instrumentation. Demands for precision to ultra-precision optical components are increasing due to advancements in optical technologies. Overall performance of optoelectronics and optomechanical systems depends on the performance of the electronic component, optomechanical assembly, and sub-micrometer geometric shape accuracies of optical components such as lenses and mirrors. Designing, fabricating, and testing intricate shapes

such as aspheres and freeforms with high surface accuracy accuracies are often challenging and time-consuming [1,2].

Computer-control optical surfacing (CCOS) processes such as sub-aperture polishing bonnet [3,4], wheel [5], magnetorheological finishing [6], laser polishing [7,8], and ion beam figuring (IBF) [9] processes are widely used to make small to large optical mirrors. A blank is shaped into the desired form and then finished from matte to specular surface in several grinding and polishing stages [10,11]. Finally, the last stage of polishing is used to achieve final design tolerances. According to the convolutional polishing model, a tool influence function (TIF) and a tool path are the two key parameters in optimizing dwell time, which is used to guide the movements of the tool during CCOS [12–14]. While a TIF describes the tool's localized correction ability per unit time during polishing, a tool path defines how the TIF travels across the workpiece to remove or reduce the surface errors during optical fabrication. The surface errors are typically categorized into form, waviness, and roughness, ranging from low-to-high spatial frequencies. While form and roughness are affected by various factors, such as machine tool wear and offsetting, envelope profiles of tool grains, tool vibrations, etc., waviness is primarily the direct consequence of tool paths.

Conventionally, in CCOS, a tool path is mapped along the clear aperture to follow a raster or spiral tool path [15]. Depending upon the error, the material is removed selectively based on the local error by dwelling tools over the region. The deterministic control of CCOS depends on the material removal rate of the sub-aperture tool [4,16]. During the polishing process, tool paths leave residual signatures caused by inherent patterns in the tool path [17]. Residual tool signatures cause waviness, which reduces the performance of the optical system [11]. Correction of these residual tool marks often requires post-polishing and smoothing cycles [1]. Randomizing the tool path helps reduce residual tool marks. Dunn *et al.* applied a pseudorandom path to reduce the effect of residual tool signatures on a hexagonal segment [18]. Wang *et al.* developed a unicursal random maze to reduce the periodic structure in the polished surface compared with the raster and Hilbert path [19]. Tam *et al.* applied and tested the peano-like tool path on the aspherical surface and demonstrated its performance [20]. It is also reported that sudden changes in velocity caused by the change in direction affect the surface during tool motion. This effect can be removed by implementing smooth bends or circular random paths, which minimizes velocity changes of the polishing tool [21]. Although these existing random tool paths reduce waviness, they are hard to be adapted to different surface shapes for localized selective correction. Polishing efficiency and accuracy are also not well considered in tool-path planning.

In this study, we propose a zonal (i.e., targeting tailored local subaperture regions with customizable aperture part boundary) Random Adaptive Path (RAP). That adds additional randomness and adapts to the local error, providing extra flexibility in handling different shapes of apertures. Moreover, based on a threshold selection of height, a surface error map is corrected in multiple passes in a cycle, reducing the overall processing time without compromising the optimization accuracy. Simulations are carried out to select threshold error using the bearing area curve and height fraction. Finally, verification of RAP is done by comparing the Peak to Valley (PV), Root Mean Square (RMS), time, and Power Spectral Density (PSD) for all combinations of three TIFs with spiral path, raster path, random path, and RAP. It has been found that RAP produces better surface quality than the spiral path with reduced processing time.

The rest of the paper is organized as follows. The RAP and selective path correction are briefly introduced in Section 2, followed by a detailed explanation of RAP generation methods in Section 3. Section 4 verifies the RAP adaptability, efficiency, and accuracy. Next, the simulated residual error is compared with spiral, raster and random polishing tool paths. Finally, the feasibility and limitations are discussed in Section 5, and Section 6 concludes the paper.

2. Zonal random adaptive path

The schematic representation of the proposed RAP is shown in Fig. 1(a), which consists of a flexible membrane (FEM)/ bonnet polishing tool, OptoTech MCP 250, engaged with the workpiece.
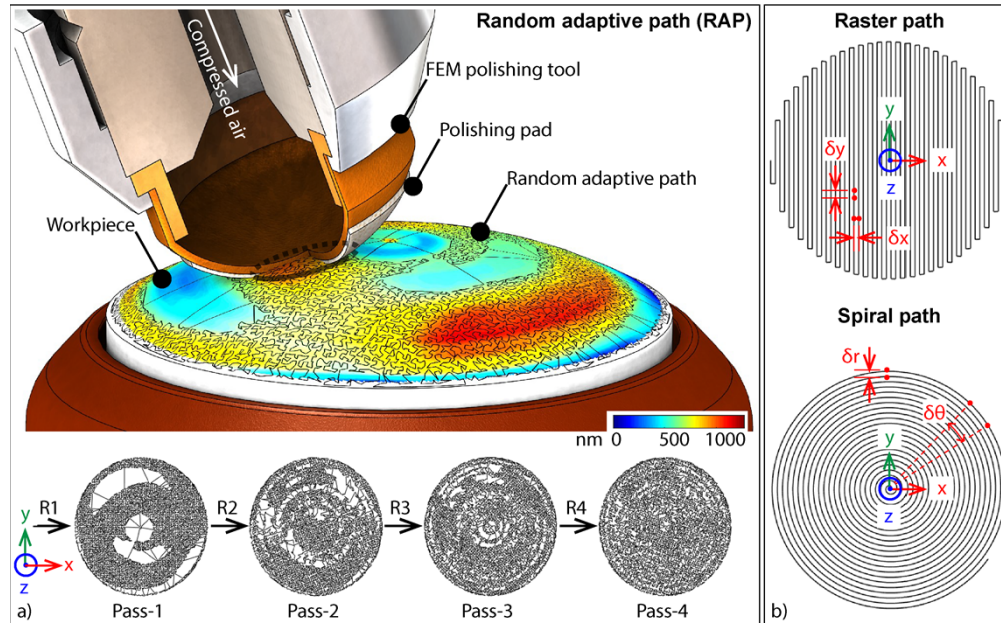

Fig. 1. (a) Schematic of the workpiece–tool interaction during CCOS and RAP for different passes (R1 to R4) in a single cycle. R1 is the initial differential surface topography, and R2, R3, and R4 are the intermediate residual error for generating RAPs; (b) conventional raster and spiral tool paths with parameters δx, δy and $\delta\theta$, δr respectively.

Existing raster and spiral tool paths are shown in Fig. 1(b). In a raster tool path, the tool meanders along x- and y-direction with point increments of δx and δy, respectively. Similarly, in a spiral path, the tool follows the Archimedes spiral path with an angular point increment of $\delta\theta$ along the arc δr. In Fig. 1(a), the RAP with a differential error map on the workpiece shows the irregularities using a color error map. Only the zonal "hot" regions above the threshold error are to be traversed during the correction cycle. Unlike the existing polishing tool paths, e.g., spiral, raster, and pseudorandom paths, random adaptive paths do correction polishing on specific subaperture zones such as convex errors shown by the yellow-red color region or skip concave error zones shown by blue regions. Example correction passes (Passes 1-4) in a cycle are shown at the bottom. Random adaptive path generation in different passes is generated using differential error maps R1-R4.

Correction polishing using a RAP is done by considering the removal threshold, i.e., the error height above which the surface is corrected in a given pass of a polishing cycle. The correction is done in multiple passes (see Fig. 1 Passes 1 to 4) with a different RAP in every pass. The RAPs for the successive multiple passes are generated using the previous pass's differential surface error maps (R1 - R4) with a given initial surface error.

This way, polishing avoids, reduces, or removes the tool path signature left during traditional polishing (spiral and raster), minimizes the polishing process time, and overlapping random paths in different passes in a single cycle enhances the surface quality of PV, RMS, and PSD. The following sections explain the random path and random adaptive path generation method.

3. Random adaptive path generation

3.1. Random path generation

The random path generation method uses a space-filling curve to obtain a base path. The generation of a base space-filling curve is systematically defined in the steps below; The base space-filling path is obtained using the Hilbert path which is based on the recursive calling of fundamental patterns. The first step is to define four basic non-terminal symbols: {H, A, B, C} as shown by the red color region surrounding the symbols H, A, B, and C in Fig. 2(a). Any non-terminal symbol is used as a starting point. Next, define a set of terminal symbols {→↓←↑} shown by blue color in Fig. 2(a). Their terminal symbol indicates the connection directly between the basic patterns during the iterations of the Hilbert curve. The levels of the curve are represented in Fig. 2(b). Finally, Replace all non-terminal symbols for constant refinement during each level. The production and replacement rules for the basic pattern and iterations are given below.

a) H←A↑H→H↓B

b) A←H→A↑A←C

c) B←C←B↓B→H

d) C←B↓C←C↑A

Fig. 2. (a) Replacement scheme of the basic pattern (A, B, C, and H) in the Hilbert curve and (b) different levels of the Hilbert space-filling curve.

To generate a random tool path with a circular part boundary, grid points along the base space-filling curve are refined to increase the point density to keep the tool path spacing less than a fraction of spot diameter [22]. Then the grid points are transformed to place the origin of the cartesian coordinate system symmetrically at the center of the regular grid of the base space-filling path. A circular part boundary is defined using the standard function used to describe the circle's equation with its center at the origin as $F(x, y) = x^2 + y^2 - R^2$. All the points outside the circle are excluded, i.e., $F(x, y) > 0$. The points inside the region of the circular part boundary, e.g., $F(x, y) < 0$, and points situated on the circumference of the circular region, $F(x, y) = 0$, remain.

Next, all the points falling near and inside the circle boundaries are extended to the boundaries of the circle. The edge effect is improved by reducing the degree in randomness near the edges

(between 0.95 to 1 times clear aperture radius) and adjusting the peripheral points to adjust near the outer boundary. This way the edge effect can be improved. Alternatively, excess of margin equivalent to the spot diameter may be considered with the diameter of work piece to avoid the edge effect. The Hilbert path in the blue circular region is shown in Fig. 3(a), and the progression of the tool path from starting 0 to finishing point 1 in Fig. 3(b). The randomized path (Fig. 3(c)) is obtained by adding random deviations from the nominal space-filling tool path, i.e., as shown in Fig. 4.

$$x_i = x_i + r\beta\delta s, \quad r \in (0, 1) \tag{1}$$

$$y_i = y_i + r\beta\delta s, \quad where\ i = 1, 2, 3 \ldots n_i \tag{2}$$

$$x_j = x_{i=k}, y_j = y_{i=k} \tag{3}$$

$$k = 1 + (j-1)\alpha, \ where\ j = 1, 2, 3 \ldots n_j\ and\ n_j = \left[\frac{(n_i - 1)}{\alpha} + 1\right] \tag{4}$$
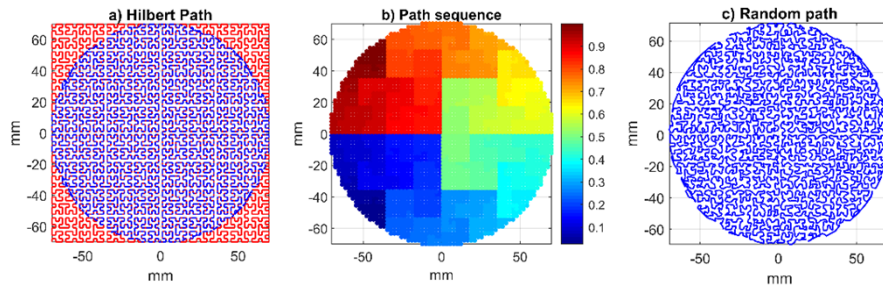
Fig. 3. Tool paths; (a) Hilbert tool path in the circular region, (b) path sequence (start 0 and stop 1), and (c) random tool path in the circular region.
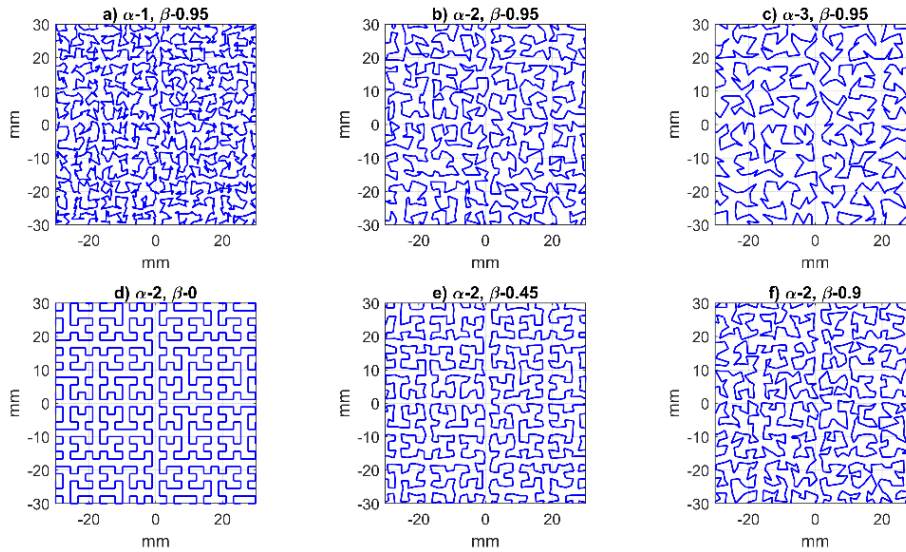
Fig. 4. Change in the tool path with reduction factor α and randomness factor β.

Randomness, β, is added to the points (x_i, y_i) inside the circular region where r is the random number, δs is the spacing between successive points in Hilbert grid space, and n_i is the total

number of points without applying reduction factor α. Here, the β was considered on the higher side, i.e., near 1, to increase the randomness. The randomness can be changed by adding a reduction factor, α, to modify the random path by alternatively reducing points in sequence. α can have an integral value of one or greater depending on the point density of initial Hilbert path or level. The base and random tool paths are shown in Fig. 3(a) and Fig. 3(c), and a random tool path with different α and β values is given in Fig. 4. As depicted, the randomness can be varied using α and β. Increasing α decreases the density of the point, and β adds randomness along with the two coordinate directions of the tool path.

3.2. Random adaptive path generation

The following steps detail the method of random adaptive tool path generation

1. As discussed in the previous section, the first prerequisite is to generate a random path over the entire aperture.

2. Select a threshold error, h_o, for generating a random adaptive tool path. The selection of h_o can be done based on mean PV error or using a bearing area curve (BAC). Differential error mapping is used for mapping the region of interest or the convex zones for correction, as shown in Figs. 5(a) and (b).

3. Omit all the tool path points in a random path below the threshold for generating the selective correction path as depicted in Figs. 5(b) and (c). Movement lines (see big lines in Fig. 5(c)) pass through the concave area. During the execution and correction of polishing, polishing tools can be dragged slowly (or lifted if the fabrication machine and tool allow) to avoid unintended micro defects from unintended polishing along these necessary connection paths. It is important to note that this zonal approach is more efficient than going through the unwanted area multiple times with a traditional path such as a spiral or raster path.

4. The sequence of polishing passes (see Fig. 1(a)) is needed based on the threshold value h_o, as shown in Fig. 6(a).
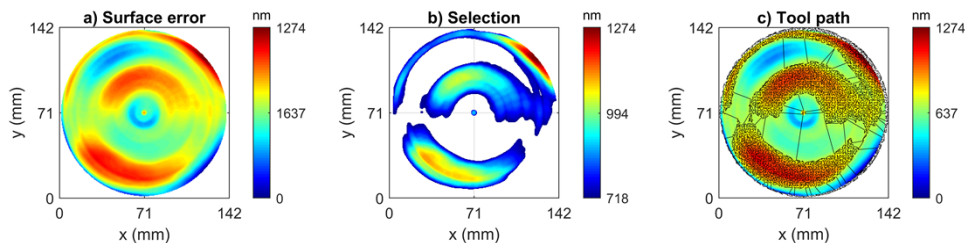

Fig. 5. (a) Surface error, (b) selective random tool path region above the threshold for correction, (c) adaptive tool path overlapping the surface error in selective areas.

This method can generate arbitrarily shaped regions, e.g., hexagon, obscured mirrors, pinwheel segments, and other usable shapes using a set of inequalities bounding the polishing path region. Compared with correcting the full aperture in one cycle, processing time can be saved in random adaptive correction polishing. Threshold error, modifying dwell time, and boundary corrections can change the time saved during random adaptive correction polishing.
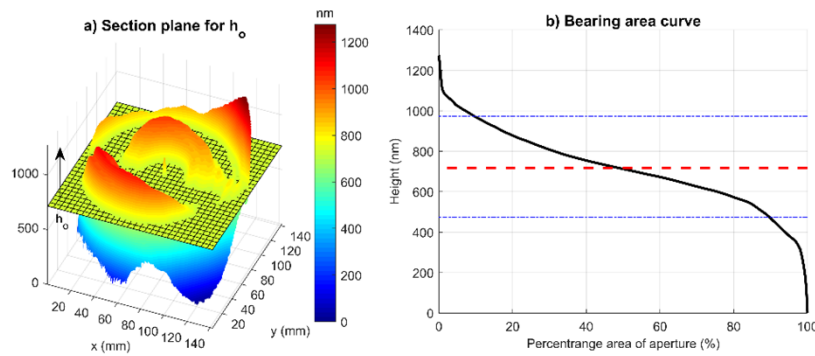
Fig. 6. (a) Differential topographic error, (b) bearing area curve.

3.3. Cutoff height for random adaptive path

Topographic error distribution is random, depending on the sequence of fabrication stages from grinding to correction polishing. Therefore, for correction using a random adaptive path, cutoff height may be selected as half, or a fraction, of the PV error within the clear aperture. Another approach is to find the areal distribution of the error within the clear aperture and use the percentage area of an aperture for random adaptive path correction in every pass. Depending on the threshold error, mid-&-high spatial frequency errors are corrected in successive polishing cycles, with low-to-mid frequency errors in initial passes and high-frequency errors in final passes.

A bearing area curve that defines the relationship between the height distribution and a percentage area function can define the cutoff height for the random adaptive correction. Figure 6(a) shows the differential topographic error with a bearing area curve (Fig. 6(b). The dotted blue lines show the height for 10% (lower dotted line) and 90% (upper dotted line) cutoff. Height up to 10% is considered the peak value, height from 90-100% of the area as valleys, and the region between 10-90% is considered core irregularities. We performed test simulations for 40%, 60%, and 80% of the percentage area of the aperture. Results are shown here in Fig. 7 a) to c) below
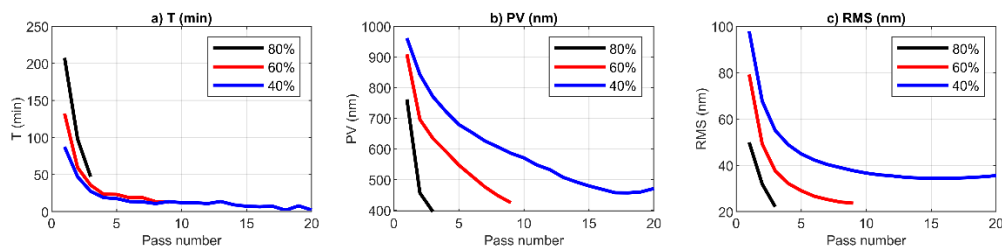

Fig. 7. (a) Process time of each pass, (b) PV (nm) error, and (c) RMS (nm) error for 40, 60, and 80% of the percentage area of the aperture.

For 40%, 60%, and 80% area, it took 20, 9, and 3 passes, respectively. With cutoff selection using a higher percentage coverage of the area, the process converges rapidly, with improved PV and RMS values compared with a cutoff selection using a lower percentage coverage area. Only a small fraction of peak errors is removed during each correction pass with lower percentage area coverage, and the number of cycles increases with low local dwell times or high feed rates. The lower percentage coverage area causes divergence at the end of correction passes due to high

instantaneous feed and low dwell time. A comparison of different cutoff cases with correction done using the spiral path and raster path in one pass is shown in Fig. 8.
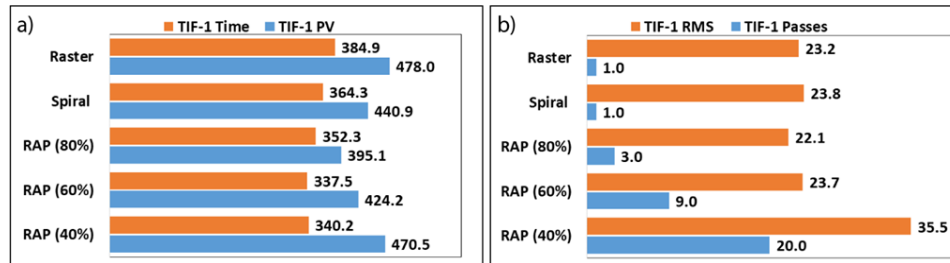

Fig. 8. Comparison of RAP with different cutoff cases with a spiral and raster paths (a) time (min), and PV (nm) (b) RMS (nm), and Passes.

4. Verification of the random adaptive path

4.1. Verification of aperture shape adaptability

Random adaptive tool path adaptability is verified in this section. Different aperture shapes and corresponding tool paths are demonstrated in Fig. 9, consisting of the random path in a circular region, a pentagon with obscuration, a hexagon with obscuration, a circular region with obscuration, a keystone segment, and a pinwheel segment [23,24]. The generation process for random paths for the circular region (Fig. 9) is given in section 3, with the $f(x,y)$ function definition of the circle coinciding with the origin. For the generation of a polygon, as shown in Figs. 9(b) and (c), a set of linear inequalities using line function $l_n(x, y)$ (where n is the nth side of a polygon) is used to constrain the region of interest in the RAP. Center obscuring was generated using the function definition of an obscuring circle $f_r(x,y)$. Similarly, the obscured circle can be obtained using $f(x,y)$ and $f_r(x,y)$. We also verified RAP adaptability to keystone and pinwheel segments. Exoplanet telescope diffracted light can be minimized using a segmented solution and a pinwheel-pupil solution using a keystone configuration. Random adaptive paths for keystone and pinwheel are given in Figs. 9(e) and (f), respectively. In the keystone segment, the random adaptive path region is bounded using functions; outside circle $f(x,y)$, obscuring circle $f_r(x,y)$, and angular limits $\theta_i \leq \theta \leq \theta_f$. In pinwheel segments, a set of four functions, inequality constraints, were used, i.e., $f(x,y)$ for outside circle, $f_r(x,y)$ for obscuring circle, $f_{\theta i}(x,y)$ for initial spoke, and $f_{\theta f}(x,y)$ for final spoke were used for bounding region within spokes and circles.

4.2. Verification of the efficiency and accuracy

Prerequisites for dwell time optimization are tool influence function, tool path, and differential topography (target removal). Spiral, raster, and random or pseudorandom paths are often used for dwell time implementation and analyses in existing processes. The systematic dwell time implementation process using a RAP is shown in Fig. 10. Where Fig. 10(a) represents the process cycle in which the initial surface error is used to evaluate the RAP, processed in a loop in several passes (p) until RMS is less than the required RMS error. RAP parameters include; threshold h_o Level L, rotation angle θ for rotation of path by a given angle in each pass, randomness β for base space-filling path, and density reduction α for reduction of point density. The dwell time optimization was carried out using the universal dwell time optimization (UDO) [14] since it allows the dwell time to be calculated for arbitrary dwell points and is computationally efficient. UDO's correction is based on selectively correcting the surface based on the tool path and thresholding the height h_o. Dwell time optimization is implemented in the region above h_o and it is optimized in every pass.
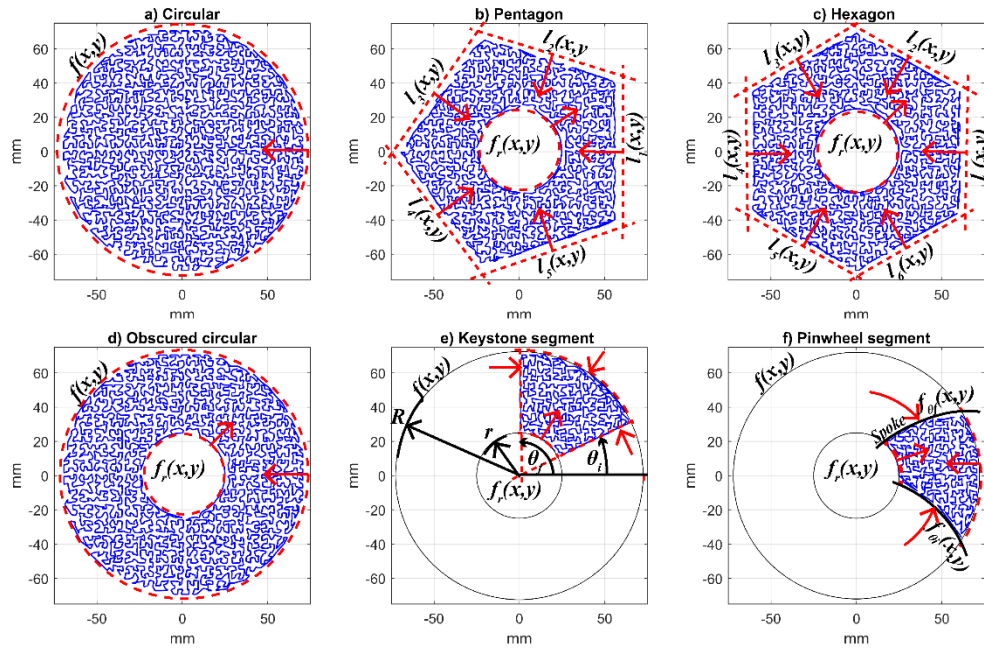
Fig. 9. Random adaptive base path verification with the geometry of shape (a) circular, (b) pentagon with obscuration, (c) hexagon with obscuration, (d) obscured circular, (e) keystone segment [24], and (f) pinwheel segment [23].
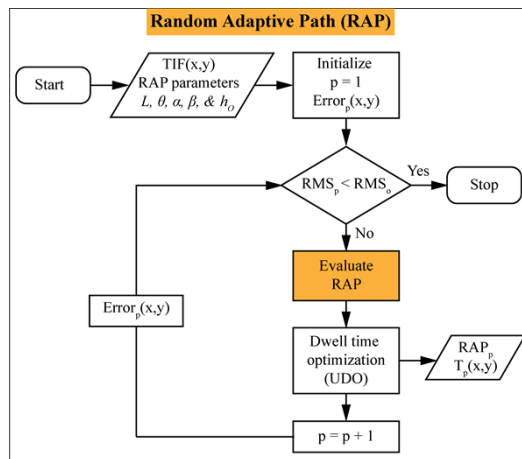

Fig. 10. Dwell time evaluation process diagram using RAP implemented with universal dwell time optimization (UDO) [14].

To study the performance of RAP, as shown in Fig. 11, three different kinds of TIFs of the FEM polishing tool from OptoTech MCP 250 [25], where the tool precessions of 0°, 5°, and 10° with Peak Removal Rates 12.75 nm/s, 28.20 nm/s, and 46.6 nm/s, respectively, are used in this simulation.
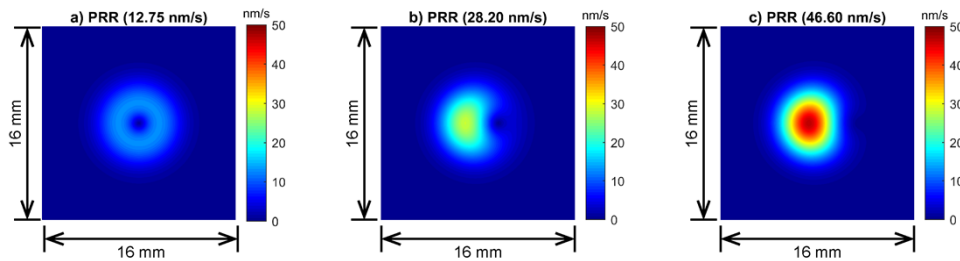
Fig. 11. TIF of polishing tool at different tool precession (ϕ) (a) TIF-1 at 0°, (b) TIF-2 at 5°, and (c) TIF-3 at 10°.

Correction polishing simulation was then performed using spiral, raster, random, and random-adaptive paths for different tool paths. UDO was used for dwell time calculation. The correction run consists of a single dwell time optimized map for the spiral, raster and random paths. In random adaptive paths, different correction runs on adaptive paths are carried in multiple passes in a single cycle based on the predetermined passes with different random adaptive paths in each pass and a path-specific dwell time map. The region for the random adaptive path was obtained using a cutoff threshold. The error above the threshold is corrected in each pass. Figure 12(a) shows the initial surface error within the 60×60 mm window of Fig. 12(b). The surface error in Fig. 12(a), tool path in Fig. 12(e), and TIF-3 (Fig. 11(c)) were used in estimating the intermediate Residual-1 in Fig. 12(i). The Residual-1 is used again in generating the path in Pass-2 for estimating Residual-2 in Fig. 12(j). The process is followed until the surface error reaches a value less than the targeted error in terms of PV or RMS. The labelled number shows the process sequence flow from (1) to (8) adjacent to the arrow from initial to final error. Other tool paths, spiral and random, are given in Fig. 12(c) and Fig. 12(d).

4.2.1. Comparison of residual error maps

Different polishing runs were carried out using TIF-1, TIF-2, TIF-3, spiral path, raster, random path, and random adaptive tool path. A general trend among different tool paths shows that PV and RMS values are lowest for random paths followed by random adaptive and spiral paths. The random adaptive path took the least time compared with spiral, raster and random. A comparison between different paths is given in Fig. 13 below.

Comparing TIF-1, TIF-2, and TIF-3, it can be depicted from Figs. 13(a) and (b) that TIF-3 achieved better results in all the cases of spiral, raster, random, and RAP in terms of processing time and RMS error. This may be due to the near Gaussian shape of the tool influence function of TIF-3. However, for a complex workpiece, it may not always be possible to engage a tool with a workpiece to create a near Gaussian-shaped TIF. Therefore, we have also considered other cases with TIF-1 and TIF-2.

Figures 14(a) to (i) shows the residual error for the different cases with different tool paths (spiral, raster, random, and RAP) along different rows and TIFs 1 to 3 along columns. For comparison, we have considered the same level of spacing for spiral, raster, random, and RAP with the same base spacing for random and RAP cases. All possible cases of three TIFs of polishing tools and tool paths, spiral, raster, and random adaptive, are given below.
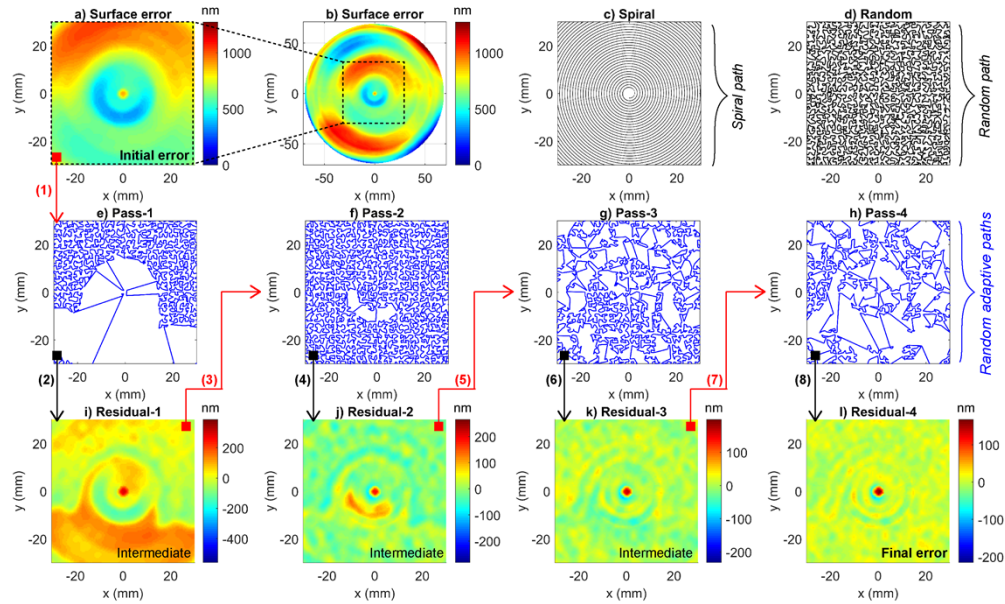
Fig. 12. (a) Initial surface error within 60×60 mm window of total surface error, (b) total surface error with different polishing tool paths; (c) spiral, (d) random, and random adaptive paths in pass-1 to pass-4 in (e) to (h) generating a respective residual error from (i) to (l).
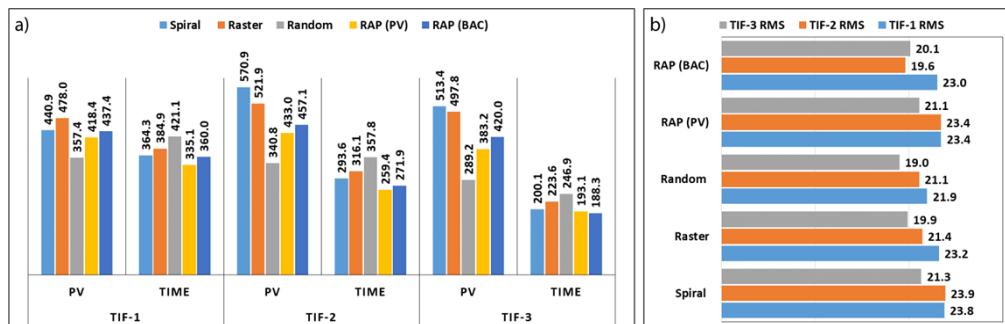

Fig. 13. Comparison of residual error for different tool paths and TIFs (a) PV (nm) and Process time (min) (b) RMS (nm).
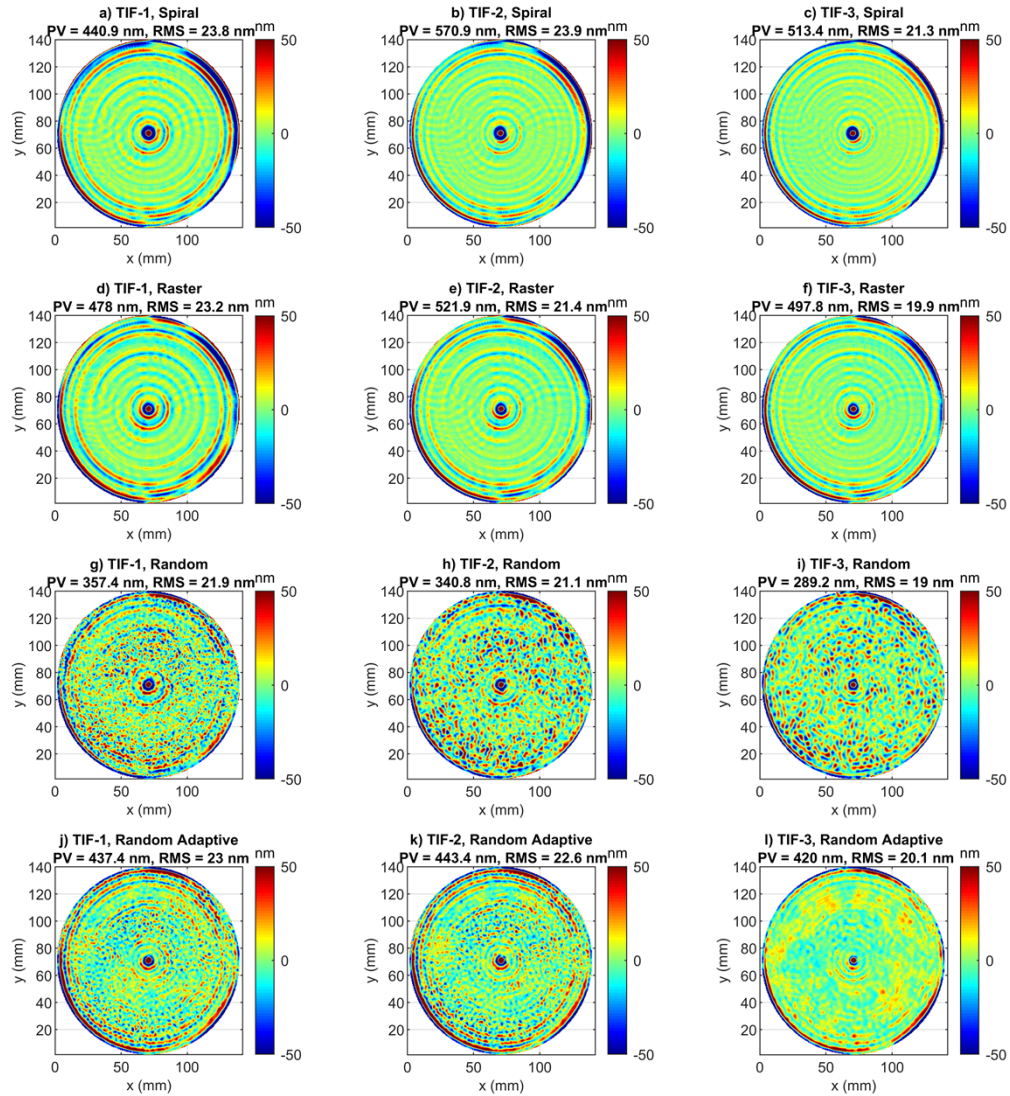
Fig. 14. Comparison grid of residual surface error for three paths, spiral, random, and random adaptive, using TIF-1, TIF-2, and TIF-3.

In the case of spiral and raster paths, residual surface errors consist of characteristic marks of spiral trajectories. These residual marks are effectively removed in the case of random and random adaptive tool paths.

4.2.2. Power spectral density analysis

Figure 15 shows the integrated PSD for different TIFs and polishing tool paths. It can be depicted from the figure for all TIF cases that random and random adaptive paths produce a low RMS distribution concerning the range of frequencies in the figure. TIF-1 shows a deviation as compared with TIF-2 and TIF-3. This may be due to the shape of TIF-1 with low central removal. For higher frequencies, similar integrated PSDs can be seen. Hence, it may be concluded from Fig. 14 and Fig. 15 that random and random adaptive paths produce better (or similar) surface quality to the traditional paths in terms of PV, RMS, and PSD. In the meantime, random adaptive paths also reduce the processing time compared to random, raster and spiral paths, while RAP enables the fabrication of various workpiece shapes to support untraditional segmentation topologies such as pinwheel segments.
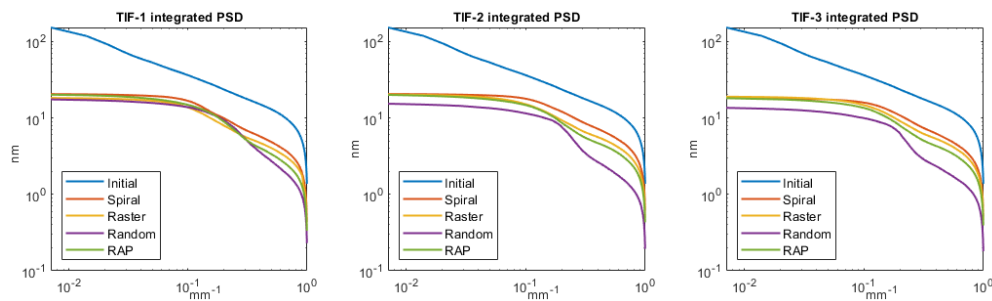

Fig. 15. Integrated power spectral density (PSD) of the final error map for different combinations of TIFs and polishing tool paths.

The PSD analysis above shows that Random path and RAP can be effectively used for removing a range of low-mid-high spatial frequency errors.

5. Discussion

Precision polishing of optics is an essential and time-consuming process. It is because, during polishing, stringent design tolerances are to be achieved. Precision polishing and finishing are generally carried out using polishing and finishing tools. The selection of a combination of polishing processes depends on the precision required and the intricacy in the shape and size of the optics. Tool influence function, tool path, and dwell time optimization are the three areas that work together to reach limiting machine performances. The correction ability of features on the surface depends on the minimum spot size used. However, reducing the spot size poses a challenge to the usable point intervals spacing or tool path spacing, especially in the case of non-contact polishing and finishing techniques, e.g., laser polishing and IBF. Therefore, randomizing the tool path is a possible solution to avoid or remove repetitive tool signatures or waviness on the surface. The proposed solution of truly randomizing ensues the non-repetitiveness in tool path patterns. During the fabrication process, the localized high amplitude of error is sensitive to handle. Full-aperture correction uses dwell time optimization in widely applied existing polishing and finishing techniques; however, tool motion is challenging to control considering machining feed limitations. Therefore, the proposed random adaptive path solution best fits such cases and polishing in general. Material removal rate and tool path density are essential factors that need to be considered during the final stages. High material removal rate with increased path density

increases correction sensitivity during the final stages, and the material removal rate must be wisely selected. Reducing the material removal rate or increasing the extra stock removal layer with increased path density may help achieve final sub-micrometer design tolerances but increase the processing time. Selective correction helps focus only on selective areas with minimum material removal rate, thereby reducing process time. This research explored the new random adaptive paths that randomize and adapt to a local error with optimized dwell time in every pass. However, we believe there is a wide scope of further optimization in selecting correction zones for adaptive correction and the development of random adaptive paths for large optical surfaces. This study kept the material removal rate low to avoid tool feed errors or feed rate problems in pseudorandom and other random paths.

In RAP, randomness β and reduction α can be adjusted to ensure the tool path avoids sharp zones. To some extent, the sharp corners can be brought close to 90 degrees by changing α and β. However, there are many points for high randomness where the tool path points are making acute angles between lines joining successive points. There is no constraint for obtuse angles, but the TIF removal rate is low to compensate for acute angle problems. Alternatively, angles between successive points can be introduced. However, it will increase complexity because it will make every angle obtuse, hampering the space-filling capacity of random paths due to a lack of sufficient bending (acute angles). The above discussion can be summarized as follows. RAP has cons in terms of limited fast tool movements due to rapid change in the direction of a tool in a random direction, which may reduce the process accuracy. On the pros side, RAP can help to selectively correct the optical surface in a single run with multiple passes, reducing mid-high spatial frequency errors and increasing surface quality. Another benefit is the ability to adapt to different workpiece boundaries as presented in prevision sections. Applying random adaptive paths for intricate shapes needs further investigation due to sensitivity in controlling multi-axis motion for complex geometries.

6. Conclusion

An innovative random path adapting to the local errors on the surface is developed, which can be used for polishing and correction polishing of differential topographic errors in a single cycle. The cycle is carried out with multiple passes enabling correction optimization in both space and time. We analyzed existing and widely used spiral and raster paths with proposed random and random adaptive paths. FEM TIF with different shapes, axis-symmetric and non-axisymmetric, was used to study the residual error PV, RMS, and PSD. A comparison shows that random adaptive paths produce better or similar surface quality overall in terms of RMS, PV, and PSD while reducing the overall process time and enabling non-traditional aperture shape fabrication.

The method may be extended to other space-filling curves. Random and random adaptive paths can be used for polishing arbitrarily shaped surfaces as verified, e.g., circular, polygon, keystone, and pinwheel full or obscured configurations. We acknowledge that the study was conducted with a randomly selected surface. Implementing random adaptive tool paths may generate errors due to tool misfits and limited axis-feed during machining complex or intricate shaped geometries if not considered in the implementation. Process time saved in random adaptive paths may vary based on the initial surface. However, random adaptive paths are helpful for rapidly converging surface error in correction stages and reducing material removal sensitivity during final correction stages by selectively correcting the surface, thereby enabling finer correction without affecting the rest of the area on the surface. Therefore, RAP is suitable for efficient commercial and precision optics fabrication using contact and non-contact sub-aperture polishing and finishing processes.

Disclosures. The authors declare no conflicts of interest.

Data availability. Data underlying the results presented in this paper are not publicly available at this time but may be obtained from the authors upon reasonable request.

References

1. D. W. Kim and J. H. Burge, "Rigid conformal polishing tool using non-linear visco-elastic effect," Opt. Express **18**(3), 2242 (2010).
2. J. P. Rolland, M. A. Davies, T. J. Suleski, C. Evans, A. Bauer, J. C. Lambropoulos, and K. Falaggis, "Freeform optics for imaging," Optica **8**(2), 161–176 (2021).
3. A. Beaucamp, Y. Namba, and P. Charlton, "Corrective finishing of extreme ultraviolet photomask blanks by precessed bonnet polisher," Appl. Opt. **53**(14), 3075–3080 (2014).
4. T. Suratwala, J. Menapace, R. Steele, L. Wong, G. Tham, N. Ray, B. Bauman, M. Gregory, and T. Hordin, "Mechanisms influencing and prediction of tool influence function spots during hemispherical sub-aperture tool polishing on fused silica," Appl. Opt. **60**(1), 201–214 (2021).
5. Z. Rao, B. Guo, and Q. Zhao, "Investigation of contact pressure and influence function model for soft wheel polishing," Appl. Opt. **54**(27), 8091–8099 (2015).
6. J. E. DeGroote, A. E. Marino, J. P. Wilson, A. L. Bishop, J. C. Lambropoulos, and S. D. Jacobs, "Removal rate model for magnetorheological finishing of glass," Appl. Opt. **46**(32), 7927–7941 (2007).
7. R. Rascher, C. Vogt, O. Fähnle, and D. Kim, "Closed-loop next generation laser polishing," in *Fifth European Seminar on Precision Optics Manufacturing*, R. Rascher and C. Schopf, eds. (SPIE, 2018), 10829, pp. 142–147.
8. J. Bliedtner, O. Faehnle, A.-M. Layher, R. Hassel, and A. Barz, "Pre-heating by defocusation of the CO_2-Laser polishing beam: an experimental report from the lab-floor -INVITED," EPJ Web Conf. **255**, 03001 (2021).
9. T. Wang, L. Huang, M. Vescovi, D. Kuhne, K. Tayabaly, N. Bouet, and M. Idir, "Study on an effective one-dimensional ion-beam figuring method," Opt. Express **27**(11), 15368–15381 (2019).
10. J. E. Harvey, N. Choi, A. Krywonos, and J. G. Marcen, "Calculating BRDFs from surface PSDs for moderately rough optical surfaces," in *Optical Manufacturing and Testing VIII*, J. H. Burge, O. W. Fähnle, and R. Williamson, eds. (SPIE, 2009), 7426, pp. 141–149.
11. J. Del Hoyo, H. Choi, J. H. Burge, G.-H. Kim, and D. W. Kim, "Experimental power spectral density analysis for mid- to high-spatial frequency surface error control," Appl. Opt. **56**(18), 5258–5267 (2017).
12. D. W. Kim and S.-W. Kim, "Static tool influence function for fabrication simulation of hexagonal mirror segments for extremely large telescopes," Opt. Express **13**(3), 910–917 (2005).
13. D. W. Kim, S.-W. Kim, and J. H. Burge, "Non-sequential optimization technique for a computer controlled optical surfacing process using multiple tool influence functions," Opt. Express **17**(24), 21850–21866 (2009).
14. T. Wang, L. Huang, M. Vescovi, D. Kuhne, Y. Zhu, V. S. Negi, Z. Zhang, C. Wang, X. Ke, H. Choi, W. C. Pullen, D. Kim, Q. Kemao, K. Nakhoda, N. Bouet, and M. Idir, "Universal dwell time optimization for deterministic optics fabrication," Opt. Express **29**(23), 38737 (2021).
15. X. Ke, T. Wang, H. Choi, W. Pullen, L. Huang, M. Idir, and D. W. Kim, "Dual-tool multiplexing model of parallel computer controlled optical surfacing," Opt. Lett. **45**(23), 6426–6429 (2020).
16. R. Pan, Y. Zhang, C. Cao, M. Sun, Z. Wang, and Y. Peng, "Modeling of material removal in dynamic deterministic polishing," Int. J Adv. Manuf. Technol. **81**(9-12), 1631–1642 (2015).
17. Z. Dong and W. Nai, "Surface ripple suppression in subaperture polishing with fragment-type tool paths," Appl. Opt. **57**(19), 5523–5532 (2018).
18. C. R. Dunn and D. D. Walker, "Pseudo-random tool paths for CNC sub-aperture polishing and other applications," Opt. Express **16**(23), 18942–18949 (2008).
19. C. Wang, Z. Wang, and Q. Xu, "Unicursal random maze tool path for computer-controlled optical surfacing," Appl. Opt. **54**(34), 10128–10136 (2015).
20. H.-Y. Tam, H. Cheng, and Z. Dong, "Peano-like paths for subaperture polishing of optical aspherical surfaces," Appl. Opt. **52**(15), 3624–3636 (2013).
21. K. Takizawa and A. Beaucamp, "Comparison of tool feed influence in CNC polishing between a novel circular-random path and other pseudo-random paths," Opt. Express **25**(19), 22411–22424 (2017).
22. X. Xie and S. Li, "Ion Beam Figuring Technology," in *Handbook of Manufacturing Engineering and Technology*, A. Y. C. Nee, ed. (Springer, 2015), pp. 1343–1390.
23. J. B. Breckinridge, J. E. Harvey, K. Crabtree, and T. Hull, "Exoplanet telescope diffracted light minimized: the pinwheel-pupil solution," in *Space Telescopes and Instrumentation 2018: Optical, Infrared, and Millimeter Wave*, M. Lystrup, H. A. MacEwen, G. G. Fazio, N. Batalha, N. Siegler, and E. C. Tong, eds., SPIE Conference Series (2018), 10698, paper 106981P.
24. D. Kim, H. Choi, T. Brendel, H. Quach, M. Esparza, H. Kang, Y.-T. Feng, J. N. Ashcraft, X. Ke, T. Wang, and E. S. Douglas, "Advances in optical engineering for future telescopes," Opto-Electron. Adv. **4**(6), 210040 (2021).
25. V. S. Negi, H. Garg, S. Kumar RR, V. Karar, U. K. Tiwari, and D. W. Kim, "Parametric removal rate survey study and numerical modeling for deterministic optics manufacturing," Opt. Express **28**(18), 26733–26749 (2020).